Theoretical Study of Interfacial Transport in Gas-Liquid Flows

Mass transfer in sheared, concurrent gas-liquid flows is investigated theoretically using solutions to the unaveraged advection-diffusion equation. For sufficiently thick films, the resistance to mass transfer is shown to be confined completely within a thin region in the liquid near the interface and mass transfer coefficients are accurately predicted by an improved numerical technique that uses a velocity field derived from an Orr-Sommerfeld equation with the time-varying velocity computed directly from measurements of interfacial waves. The mass transfer coefficients are shown to depend on the magnitude and frequency content of the velocity fluctuations normal to the interface. As the film thickness decreases, transfer resistance extends throughout the film and turbulent mixing in the middle of the film controls the transfer rates. For this region, limiting values of transfer coefficients are predicted well by analytical solutions to the advection-diffusion equation, which assume a laminar flow.

D. D. Back, M. J. McCready
Department of Chemical Engineering
University of Notre Dame
Notre Dame, IN 46556

Introduction

Overview

For the absorption of slightly soluble gases or the condensation of a pure vapor onto a subcooled liquid, the primary resistance to transport lies in the liquid phase and as a consequence, transfer rates are controlled by the liquid velocity field in the near vicinity of the interface. At the interface a thin (as small as 10^{-4} m for a sheared gas-liquid interface) concentration or thermal boundary layer will occur in which a balance exists between convective and diffusive modes of transport. If the flow is irregular in space and time, it is expected that the effectiveness of individual velocity fluctuations on mass (or heat) transfer will depend upon their size and duration as well as their magnitude. The resulting average transport rate and the temporal and spatial scales of the concentration fluctuations will be the result of the combined effects of forcing due to velocity fluctuations and smoothing caused by diffusion. Time-averaged advection-diffusion equations that use eddy diffusivities to account for scalar convection cannot accurately describe this balance because they neglect the inherent dynamical nature of the problem.

Efforts to achieve an understanding of the diffusion-convection balance and exactly how the fluctuating flow field controls mass transfer have been limited by the small size of the region, which prevents direct measurements of either the velocity fields or the concentration fields. Until these experimental limitations are overcome, research to improve the understanding of the basic physics of interfacial mass transfer must rely on solutions, either analytical or numerical, of the governing mass balance equation using the best available representations for velocity fields.

In the present paper, absorption of a slightly soluble component from a turbulent gas flow into a sheared liquid film where the surface is covered by nonbreaking waves is examined. These films exhibit mass transfer rates that are generally an order of magnitude larger than those for unsheared films. In order to understand the reason for these increased rates, one must consider the hydrodynamics in the vicinity of the interface resulting from the interaction of surface waves with the turbulent gas flow, as well as velocity fluctuations which are part of the bulk flow of the liquid.

Figure 1 depicts the gas-liquid flows to be discussed. Concurrent (or countercurrent) gas flows over waves existing at the surface produce mean and fluctuating shear stresses. The mean shear stress τ at the interface is related to the friction velocity v^*, by $\tau = \rho_L v^{*2}$, where ρ_L is the liquid density. The interfacial concentration of the solute is c_i^*. Slightly soluble solute $\mathcal{A}$ desorbs or absorbs into a liquid film of dimensionless thickness m, characterized by a Schmidt number, Sc, of order 10^2 or greater. The Schmidt number is defined as ν/D, where ν is the liquid kinematic viscosity and D the molecular diffusivity of $\mathcal{A}$ in the liquid. The gas flow is highly turbulent, with a gas Reyn-

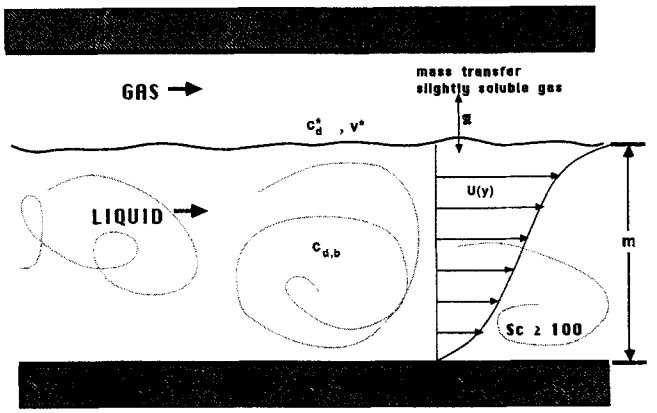

Figure 1. Gas-liquid flow diagram.

olds number Re_G typically of order 10^4, and the film hydrodynamics will be comprised of a spectrum of secondary flows superimposed on a mean velocity profile, $U(y)$. It is the magnitude and frequency content of the secondary flow field that will transiently distort the concentration boundary layer region to produce mass transfer rates larger than the pure diffusional values.

Previous work

Experimental studies. The absorption of a slightly soluble gas into a liquid sheared by concurrent gas flow has been studied experimentally by numerous investigators. Mattingly (1977), Aisa et al. (1981), McCready and Hanratty (1985), Henstock and Hanratty (1979), Kasturi and Stepanek (1974), and Chung and Mills (1974), to name a few, have measured absorption rates to highly sheared liquid flows in horizontal or vertical orientations. The results for $40 < m < 700$ may be summarized as

$$0.1 < K\,Sc^{1/2} < 0.2 \tag{1}$$

where K is the average mass transfer rate made dimensionless with the liquid-side friction velocity and m is the film thickness made dimensionless using the friction velocity and the kinematic viscosity. It is noted that for many of the individual data sets, K changes very little with m. The range of K in Eq. 1 is due mainly to disagreement among different investigations as to the value of this asymptote. As mentioned above, these rates are typically about an order of magnitude larger than an analogous film without gas shear.

Very similar behavior has been observed by Jensen and Yuen (1982) for the condensation of steam onto a subcooled, concurrently flowing liquid layer. Their data can be summarized by

$$0.1 < H\,Pr^{1/2} < 0.2 \tag{2}$$

where H is the average heat transfer coefficient scaled with the friction velocity and Pr is the Prandtl number. The transfer coefficient ranges of Eqs. 1 and 2 are nearly identical, and it is therefore very possible that similar mechanisms control the scalar transport process. This result is surprising since Sc is ordinarily much greater than 10^2 so that the concentration boundary layer region is confined to a very thin region near the interface, whereas with Pr typically between 10^0 and 10^1, the thermal boundary layer will extend much farther from the interface.

Studies to determine the interfacial hydrodynamics have been limited by the presence of interfacial waves. The velocity field measurements of Caussade and Souyri (1986) and Fabre et al. (1984) have revealed some bulk hydrodynamic properties, but the flow field in the interfacial region has not been experimentally characterized. The origin of velocity fluctuations and their role in enhancing mass transfer rates over pure diffusional values must consequently be inferred from intuition and a physical understanding of the processes that occur near the surface. Many investigators have speculated that the source of important velocity fluctuations is due to wall- or interfacially generated turbulence, or possibly wave-induced mixing, and have developed conceptual models for use in interpreting measured rates. A decade ago, Henstock and Hanratty (1979) reviewed much of the literature up to that point. Their analysis of the various models indicated that almost all were capable of fitting experimental data with reasonable degrees of success but that no definitive predictive procedure was available that would calculate mass transfer coefficients from hydrodynamic information alone.

McCready and Hanratty (1985) noted that variation in interfacial shear stress caused by a turbulent gas flow over small-wavelength waves induced velocity fluctuations in the liquid at close proximity to the interface. If these fluctuations are sufficiently strong, they can be quite effective in enhancing mass transfer. The shear stress measurements and theoretical predictions of Thorsness et al. (1978) and Abrams and Hanratty (1985) for flow over a solid wave train, which indicate that the stress variation may be as large as 50% of the average stress for even small-amplitude waves, were used to evaluate this mechanism. Values of the magnitude of the induced velocity fluctuations appeared to be greater than fluctuations caused by turbulent eddies approaching the interface or oscillations caused by wave motions. The application of these solid-liquid wave shear stress measurements to gas-liquid waves should be a good approximation since the liquid-to-gas viscosity ratio is of order 10^2. Hanratty (1983) has shown that the use of these values to describe gas-liquid interfacial conditions in linear stability analyses produces good predictions of the point of incipient stability as well as the fastest growing wavelengths.

Mass transfer rates measured by Aisa et al. (1981), Henstock and Hanratty (1979), and McCready and Hanratty (1985) may be schematicized as in Figure 2, which depicts a change in mass transfer rate behavior around $m = 40$. This corresponds to a liquid Reynolds number, Re_L, based on four times the film thickness, of about 1,750. In region I of Figure 2, rates are approximately given by the relation of Eq. 1. These rates are characterized by an invariance as the dimensionless film thickness m increases. Since Re_L increases with m, the film becomes increasingly turbulent as m increases. However, the mixed state of the film apparently offers no resistance to scalar transport and changes in the bulk turbulence do not affect the mass transfer rates. Mass transfer coefficients scale with the degree of interfacial shear and the major transport resistance will be through the very thin concentration boundary layer region near the interface. Consequently, a complete description of mass transfer in this region can be obtained by study of the behavior within the concentration boundary layer.

For thinner films, regions II and III in Figure 2, mass transfer rates decrease by as much as an order of magnitude. The drop-

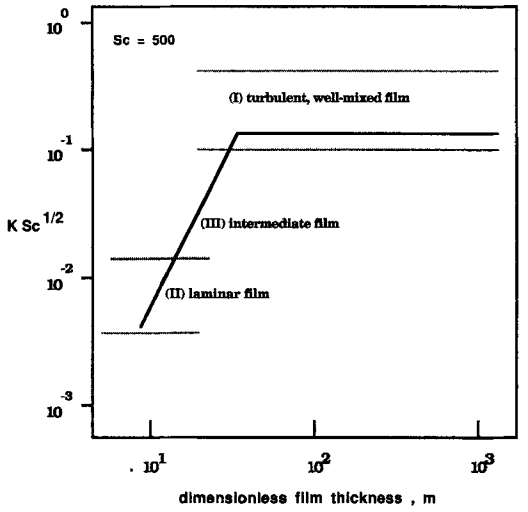

Figure 2. Average mass transfer rate (K) regimes as a function of dimensionless film thickness m.

off with m is undoubtedly a result of the suppression of secondary flows in the film, which must approach laminar film behavior. Solutions of the two-dimensional, steady state advection-diffusion equation for mass have been carried out by several researchers for different flow configurations to investigate the nature of laminar film mass transfer. In the present study, eigenvalue solutions similar to those of Rotem and Neilson (1969) are formulated for the flow field of Figure 1.

Numerical and Analytical Studies. In a series of papers, Stewart and coworkers (Stewart, 1963, 1987; Stewart et al., 1970; Stewart and McClelland, 1983) have investigated convective heat and mass transfer by examining analytical solutions of the advection-diffusion equations for numerous flow configurations. Their solutions demonstrate the effect of various properties of the velocity field on mass transfer rates. For situations where the controlling velocity field is known, good qualitative and in some cases quantitative predictions of transfer rates are achieved. This work clearly shows that it is appropriate to use balance equations as a basis for all theoretical investigations of mass or heat transfer because better characterization of the fundamental behavior can be determined from solution of the governing equation than from conceptual models.

From the work of Polhausen (1921), it can be seen that solutions of the advection-diffusion equation are greatly simplified for large Schmidt number because the concentration boundary layer thickness, δ_c, will be very thin relative to the hydrodynamic boundary layer thickness, δ_h. As a consequence, the velocity field in the interfacial region may be approximated as a truncated Taylor series expansion about the interface. Numerical simulations of mass transfer at a solid-liquid interface have been done by Brodkey et al. (1978) and Campbell and Hanratty (1983) and at a gas-liquid interface by McCready et al. (1986). In all these studies the advection-diffusion equation was solved for a finite domain corresponding to the concentration boundary layer with the thickness of the domain being chosen more or less arbitrarily, as it was thought that its value did not significantly affect the computations. However, Back and McCready (1988) recognized that the value chosen for the concentration boundary layer thickness does influence the computations and they provided an unambiguous procedure for choosing it. They note that because the average total flux is not a function of distance from the boundary, the time-and-space averaged value of the diffusive flux at the interface must equal a similarly averaged value of the convective flux at the outer edge of the concentration boundary layer where net diffusion is negligible.

The interest of the present study is to explain the interfacial mass transfer behavior observed for cocurrent gas-liquid flows, Figure 2, and to address several general issues that arise in turbulent mass transfer. From measurements of wave amplitude spectra, the interfacial stress, and knowledge of the flow rates and depths of the two phases, accurate and direct computation of mass transfer rates at a gas-liquid interface is done. The velocity field used in the finite difference solutions is computed from reconstructions of the interface shape obtained by inverse-Fourier-transforming the wave spectra and performing an analytic solution of an Orr-Sommerfeld equation that incorporates the shear stress variation due to gas flow over interfacial waves. By comparing one- and two-dimensional solutions of the unaveraged advection-diffusion equation for mass, the velocity component normal to the interface is found to exert a dominant contribution to mass transfer. As a result, mass transfer rates are found to be a strong function of the normal velocity statistical properties very near the interface. With no adjustable parameters, numerical predictions of mass transfer coefficients are found to agree quite well with measurements for thick films—region I of Figure 2. The limiting behavior of mass transfer rates for thinner films is also predicted from an eigenvalue solution of a horizontal laminar film.

Theoretical Development

Film physics

Figures 3a and 3b show the hypothesized difference between a thick, well-mixed film and a near-laminar film, respectively. In Figure 3a, the bulk is completely mixed to some dimensional homogeneous concentration $c_{d,b}$ (it should be noted that δ_c has been greatly exaggerated in this figure). The bulk concentration will extend throughout the film, except within the concentration boundary layer near the gas-liquid interface. Of particular concern is the behavior of mass transport at the gas-liquid interface. The concentration boundary layer at this interface, δ_c, will be the dominant resistance to absorption or desorption if the film is sufficiently mixed. Since δ_c is very thin, normal velocity fluctuations generated right at the interface should be extremely effective in enhancing mass transport to and from the interface. The cellular flow field set up by shear stress variations, τ', over the waves is sketched for an instant in time.

For thinner films, the secondary flows will dissipate and the film will no longer be homogeneously mixed. The concentration and hydrodynamic boundary layers will then begin to encompass the entire film, as illustrated in Figure 3b. Accordingly, to understand mass transport to these films a study of the entire film is necessary.

Interfacial mass transport in turbulent well-mixed films

Because measurements of surface waves present at sheared gas-liquid interfaces reveal that the amplitude-to-wavelength ratio a/λ is of order 10^{-3}–10^{-1}, and from mass transfer measurements the concentration boundary layer thickness is esti-

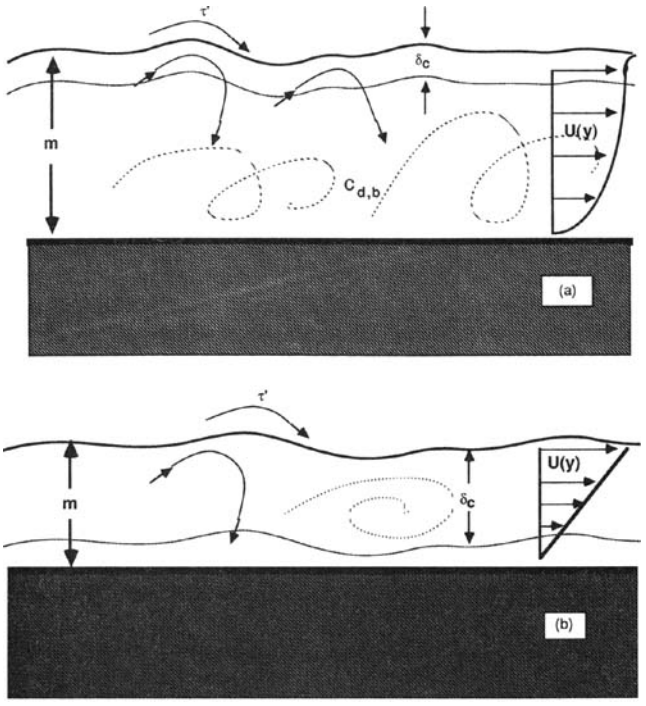

Figure 3. Gas-liquid flow.
(a) Turbulent well-mixed film
(b) Thin near-laminar film

mated to be typically much less than 10^{-3} m, the effect of curvature will be neglected. In addition, the time scale for the flow within the waves which causes the scalar transfer relative to the interface is much shorter than any evolution (e.g., growth or decay of waves) so that waves can be viewed as steady traveling forms that propagate without change of shape. Under these conditions, it is appropriate to formulate the problem using a coordinate system located on the interface and moving with the average tangential speed of the interface.

The concentration field is related to hydrodynamics through the advection-diffusion equation for mass:

$$\frac{\partial c}{\partial t} + \nabla \cdot (\boldsymbol{u}c) = \frac{1}{Sc}\nabla^2 c. \tag{3}$$

The dimensionless concentrations $c(x, y, z, t)$ is defined as $(c_d - c_{d,b})/(c_d^* - c_{d,b})$, where c_d^* is the dimensional interfacial concentration, $c_{d,b}$ is the bulk concentration, and $c_d = c_d(x, y, z, t)$. All other variables in the foregoing discussion are made dimensionless with the liquid interfacial friction velocity and ν, the kinematic viscosity. The vector $\boldsymbol{u}$ is the velocity field (u, v, w), t is time, and the coordinate system is oriented such that y is normal to the interface and increasing into the liquid, and x denotes the tangential, or flow, direction. The dimensionless convective mass transfer coefficient, k, is defined as

$$k = \frac{1}{Sc}\left(\frac{\partial c}{\partial y}\right)_{y=0} \tag{4}$$

From Eq. 3, k will be a function of Sc and the magnitude and frequency of individual velocity fluctuations that thicken and thin the boundary layer region.

Equation 3 is linear in concentration. As a consequence, it should be possible to define average properties of the concentration which depend upon the statistical behavior of the forcing velocity field and not on specific instantaneous events or initial conditions. The velocity fluctuations that control mass transfer are expected to be related to the wave surface properties through the velocity field in the immediate vicinity of the interface. Therefore, a mass transfer coefficient based on the average interfacial concentration gradient, which is also the temporal and spatial average of k, can be determined from statistical properties of the velocity field as

$$K = f\,[\underline{\beta}^2(a, f, \chi, \lambda), f_c(a, f, \chi, \lambda), Sc] \tag{5}$$

where $\underline{\beta}^2$ is a characteristic variance, or "energy," of the interfacial velocity field, and f_c is a characteristic frequency (which should represent a frequency range of dominance in the hydrodynamic field), each a function of the wave amplitude a, frequency f, speed χ, and wavelength λ. It is noted that the nature of the function f must be determined by solution of Eq. 3.

A two-dimensional surface is assumed, noting the possible extension to a three-dimensional regular surface by Squire's (1933) transformation. In the moving coordinate the resultant two-dimensional velocity field condenses to the fluctuations $u'(x, y, t)$ and $v'(x, y, t)$, and Eq. 3 reduces to

$$\frac{\partial c}{\partial t} + \frac{\partial (v'c)}{\partial y} + \frac{\partial (u'c)}{\partial x} = \frac{1}{Sc}\left(\frac{\partial^2 c}{\partial y^2} + \frac{\partial^2 c}{\partial x^2}\right) \tag{6a}$$

The boundary conditions employed for a solution are

$$\text{at } y = 0, \quad c = 0 \tag{6b}$$

$$\text{at } y = \delta_c, \quad c = 1 \qquad \text{for } v'(x, y, t) < 0$$
$$\partial c/\partial y = 0 \quad \text{for } v'(x, y, t) > 0 \tag{6c}$$

$$\text{at } x = 0, \quad \partial c/\partial x = 0 \tag{6d}$$

$$\text{at } x = x_L, \quad \partial c/\partial x = 0 \tag{6e}$$

The computer time required for solution of this problem could be greatly reduced if Eq. 6a were reduced to

$$\frac{\partial c}{\partial t} + \frac{\partial (v'c)}{\partial y} = \frac{1}{Sc}\frac{\partial^2 c}{\partial y^2} \tag{7a}$$

with the boundary conditions of Eqs. 6b and 6c. As written, Eq. 7a violates the continuity equation. However, Stewart et al. (1970) demonstrated that the influence of the normal component of the velocity field on the resulting transfer rate is much greater than the tangential component. Also, Campbell and Hanratty (1983) found that Eq. 7a gave essentially the same behavior as a two-dimensional equation. It is of interest to determine why this occurs. Consequently, numerical simulations using both Eq. 6a and Eq. 7a will be compared.

The boundary condition of Eq. 6c (previously used by Campbell and Hanratty, 1983) is used because of its physical significance when viewing the concentration boundary layer as a separate entity from the bulk at concentration $c = 1$. That is, bulk fluid of concentration $c = 1$ enters the region δ_c during an inflow

toward the interface. During an outflow from the interface, the concentration is not known at the edge of δ_c and $\partial c/\partial y$ is expected to vanish.

In order to solve Eq. 6 or 7, it is necessary to define δ_c in a consistent and plausible manner. This can be done by recognizing that the time-averaged mass flux at $y = \delta_c$ is due almost completely to convection (because the concentration gradient is very close to zero) and must equal the interfacial flux, which is caused by pure diffusion. Since the convective flux is monotonically increasing (until it reaches the value of the diffusive flux at the interface) away from the interface, δ_c can be defined as the smallest y at which the convective flux is equal (within 1%) to the interfacial flux.

Allowing c to be composed of an average and fluctuating part, $c = C + c'$, the time averages of Eqs. 6a and 7a are

$$\frac{\partial\langle v'c'\rangle}{\partial y} + \frac{\partial\langle u'c'\rangle}{\partial x} = \frac{1}{Sc}\left(\frac{\partial^2 C}{\partial y^2} + \frac{\partial^2 C}{\partial x^2}\right) \tag{8}$$

and

$$\frac{\partial\langle v'c'\rangle}{\partial y} = \frac{1}{Sc}\frac{\partial^2 C}{\partial y^2} \tag{9}$$

where $\langle\ \rangle$ denotes a time-averaged product. If Eqs. 8 and 9 are integrated over δ_c, defined from the region where diffusion dominates ($v' = 0$ at $y = 0$) to the region in which convection dominates ($\partial c/\partial y \approx 0$ at $y = \delta_c$), the result is

$$K(x) = -\langle v'c'\rangle_{y=\delta_c} - \int_0^{\delta_c}\left(\frac{\partial\langle u'c'\rangle}{\partial x}\right)dy + \frac{1}{Sc}\int_0^{\delta_c}\left(\frac{\partial^2 C}{\partial x^2}\right)dy \tag{10}$$

$$K = -\langle v'c'\rangle_{y=\delta_c} \tag{11}$$

These equations are interpreted as a balance between diffusive and convective fluxes, and are used in numerical solutions to define both δ_c and the average mass transfer coefficient, K. In two dimensions, K is defined as the average of $K(x)$, Eq. 10, over x. It is noted that because the bulk concentration is changing very slowly in the x-direction, the value of δ_c in Eq. 10 is constant with x.

For large Sc, δ_c is very thin and completely contained within the hydrodynamic layer, δ_h. The velocities will be approximated by a Taylor series expansion about the interface, $y = 0$:

$$v'(x, y, t) = v'_{y=0} + y\left(\frac{\partial v'}{\partial y}\right)_{y=0} + O(y^2) \tag{12}$$

and

$$u'(x, y, t) = u'_{y=0} + y\left(\frac{\partial u'}{\partial y}\right)_{y=0} + O(y^2) \tag{13}$$

Truncating to one expansion term and noting that $v'_{y=0}$ is the surface wave normal velocity, the velocity field within the surface of the liquid is expressed as

$$v'(x, y, t) = y\left(\frac{\partial v'}{\partial y}\right)_{y=0} \equiv \beta(x, t)y \tag{14}$$

and

$$u'(x, y, t) = u'_{y=0} \equiv \gamma(x, t) \tag{15}$$

In accordance with the preceding discussion, the statistical properties of $\beta(x, t)$ will be of primary interest when studying and understanding the behavior of Eq. 6a or 7a.

Velocity field for thick, well-mixed films

The discussion and formulation to this point are valid for any velocity field present in the thin interfacial region within a surface wave. For the present work, the interaction of the turbulent gas flow and the waves is assumed to be causing the velocity fluctuations that will control the mass transfer rate. Velocity fluctuations due to bulk turbulence and wave mixing effects are thought to be of much lesser magnitude near the interface and to act only to mix the film far away from the interface. In addition, consistent with studies of waves by Cohen and Hanratty (1965) and Gastel et al. (1985), the effect of turbulence on the Orr-Sommerfeld formulation is also neglected. The good agreement with experimental growth rates and linear wave speeds observed in their studies provides adequate justification for this approximation.

Because the concentration gradient is confined to a very thin region near the interface where inertial effects are expected to be small and the wave slopes (i.e., a/λ) are also small, the velocity field used in the calculations will be constructed from a linear superposition of waves. As shown by Back and McCready (1988), such a velocity field can be formulated from an Orr-Sommerfeld equation:

$$-i\alpha[\chi - U(y)]\left(\frac{d^2F}{dy^2} - \alpha^2 F\right) - i\alpha FU'' = \frac{d^4F}{dy^4} - 2\alpha^2\frac{d^2F}{dy^2} + \alpha^4 F \tag{16}$$

The function $F(y)$ has been defined from a two-dimensional continuity equation with

$$v'(x, y, t) = -i\alpha F(y)e^{i\alpha(x-\chi t)} \tag{17}$$

and

$$u'(x, y, t) = \frac{dF(y)}{dy}e^{i\alpha(x-\chi t)} \tag{18}$$

Solutions to Eq. 16 given by Cohen and Hanratty (1965) and Gastel et al. (1985) for large $\alpha m^2\chi$ consist of two viscous and two inviscid parts and are written as:

$$F(y) = A_1e^{\alpha y} + A_2e^{-\alpha y} + A_3G_3(y)e^{sy} + A_4G_4(y)e^{-qy} \tag{19}$$

with

$$G_3(y) = 1 - i\alpha U'(0)(5ys^{-2} + y^2s^{-1})/4 + \cdots$$

and

$$G_4(y) = 1 + i\alpha U'(m)[5(m-y)q^{-2} - (m-y)^2q^{-1}]/4 + \cdots$$

where $i = (-1)^{1/2}$, $q^2 = -i\alpha\chi$, and $s^2 = -i\alpha[\chi - U(0)]$. The complex roots of s and q are chosen so that ***Real*** $[(q^2)^{1/2}] < 0$ and ***Real*** $[(s^2)^{1/2}] < 0$. The boundary conditions descriptive of the gas-liquid system are the *kinematic condition* at the interface, a gas-liquid *shear stress match* at the interface, and the *no slip* condition at the solid boundary. In mathematical form, these boundary conditions are

$$\text{at } y = 0, \quad F = a[\chi - U(0)] \tag{20a}$$

$$\text{at } y = 0, \quad F''(0) + \alpha^2 F(0) = \tau(0) \tag{20b}$$

$$\text{at } y = m, \quad F(m) = 0 \tag{20c}$$

$$\text{at } y = m, \quad F'(m) = 0 \tag{20d}$$

respectively. The variable $\tau(0)$ is the magnitude of the shear stress variation (SSV) at the interface; its value will determine the strength of the normal velocity fluctuations. Upon solving for the constants A_k, $\beta(x, t)$ and $\gamma(x, t)$ of Eqs. 14 and 15 may be rewritten as

$$\beta(x,t) = -i\alpha\{\alpha(A_1 - A_2) + A_3[s - i\alpha 5U'(0)s^{-2}/4] + -A_4[q + i\alpha U'(m)(5q^{-2} + 3mq^{-1} - m^2)/4]\}e^{i\alpha(x-\chi t)} \tag{21}$$

$$\gamma(x,t) = \frac{i}{\alpha}\beta(x,t) \tag{22}$$

with ***Real*** (Eq. 21) and ***Real*** (Eq. 22) being the velocity field used in solutions of the advection-diffusion equation. It can easily be verified that the constants A_k all involve $\tau(0)$ in the numerator, which greatly affects the magnitude of β^2. As suggested by Eq. 5, this velocity field is a function solely of wave parameters a, α, and χ since $\tau(0) = a \cdot f(\alpha^p)$, where $p > 0$. The surface spectral parameters a, α, and χ are computed with a measured wave amplitude spectrum utilizing a dispersion relation discussed in detail by Back and McCready (1988).

Interfacial mass transport for laminar films

The obvious lower limit on transfer rates is a laminar, nonwavy film. For this case, analytical predictions of mass transfer rates are possible. Previously, Eq. 3 has been scaled with the appropriate hydrodynamic scales near the interface, v^* and ν. For a laminar film, the bulk fluid is not completely mixed at some homogeneous concentration. Consequently, the hydrodynamics of the entire film influence the concentration field, and Eq. 3 should be rescaled with more relevant film variables, m and $U(0)$. Film thickness data presented by McCready and Hanratty (1985) suggest that the velocity profile for a thin, sheared film at low Reynolds numbers should be nearly linear. Assuming a linear mean velocity profile, $U(y) = U(0)(1 - y/m)$, and no secondary flows, Eq. 3 becomes

$$\eta\frac{\partial c}{\partial \zeta} = \frac{1}{Pe}\left(\frac{\partial^2 c}{\partial \zeta^2} + \frac{\partial^2 c}{\partial \eta^2}\right) \tag{23}$$

where $\eta = (1 - y/m)$, $\zeta = x/m$, and $Pe = [Sc\, U(0)m]$. Equation 23 is expected to govern very thin films in which the secondary flow patterns have dissipated, and a concentration gradient extends throughout the film.

The boundary conditions ascribed to Eq. 23 are

$$\text{at } \zeta = 0, \quad c(0, \eta) = c_0 \tag{24a}$$

$$\text{at } \zeta = \infty, \quad c(\infty, \eta) = 0 \tag{24b}$$

$$\text{at } \eta = 1, \quad c(\zeta, 0) = 0 \tag{24c}$$

$$\text{at } \eta = 0, \quad \partial c/\partial\eta = 0 \tag{24d}$$

Following the method of Rotem and Neilson (1969), who solved the case of a parabolic profile, the eigenvalue solution to Eq. 23 which satisfies the far-field film saturation condition, Eq. 24b, is

$$c(\zeta, \eta) = \sum_{k=0}^{\infty} B_k H_k(\eta) e^{-\lambda_k \zeta/Pe} \tag{25}$$

where $H_k(\eta)$ are the eigenfunctions, and λ_k are the eigenvalues. Applying the remaining boundary conditions, $H_k(\eta)$ is found in terms of the Airy functions and their derivatives, ***Ai***, ***Bi***, and ***Ai'***, ***Bi'***, respectively. The solution is written as

$$H_k(\eta) = \boldsymbol{Ai}[\theta(\eta)] - \frac{\boldsymbol{Ai}'(\mu)}{\boldsymbol{Bi}'(\mu)}\boldsymbol{Bi}[\theta(\eta)] \tag{26}$$

where

$$\theta(\eta) = -\lambda_k^{1/3}\left\{\eta + \frac{\lambda_k}{Pe^2}\right\} \tag{27}$$

and

$$\mu = -\frac{\lambda_k^{4/3}}{Pe^2} \tag{28}$$

The characteristic equation is

$$0 = \boldsymbol{Ai}[\theta(1)] - \frac{\boldsymbol{Ai}'(\mu)}{\boldsymbol{Bi}'(\mu)}\boldsymbol{Bi}[\theta(1)] \tag{29}$$

and the constants B_k are given as

$$B_k = \frac{\int_0^1 H_k[\theta(\eta)]\theta(\eta)c_0\, d\eta}{\int_0^1 H_k[\theta(\eta)]^2\theta(\eta)\, d\eta} \tag{30}$$

For a typical solution, 10 to 20 terms in Eq. 25 are used such that $c(\zeta, \eta)$ varied by no more than 0.01% with the next expansion term. Figure 4 shows concentration profiles calculated for

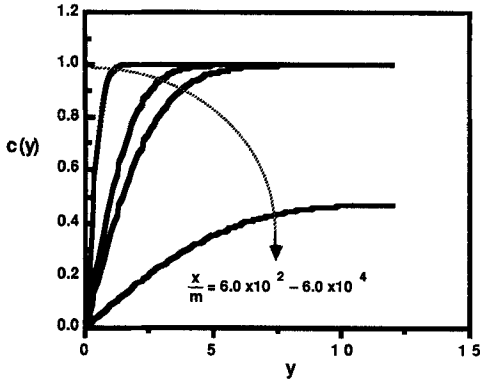

Figure 4. Average concentration profiles in y for different x, computed from Eqs. 24–25.
$Pe = 7.25 \times 10^4$; $U(0) = 10.4$; $m = 12.0$; $Sc = 580$

$Pe = 7.25 \times 10^4$, $U(0) = 10.4$, $m = 12.0$, and $Sc = 580$. As expected, these profiles display the increasing saturation ($c \rightarrow 0$) of a film as the distance from initial contact with $\mathcal{A}$ increases.

Numerical Solution for Well-mixed Films

Velocity field construction

The velocity field given by Eqs. 17 and 18 is a function of one particular set of Fourier component wave parameters. Since the actual wave surface will be composed of numerous wave spectral sets, any velocity field associated with these wave properties will also be composed of numerous sets. For the region very near the interface where the resistance to mass transfer is located, viscous forces will dominate inertia and it will consequently be assumed that the velocity field can be expressed by a superposition of the effects of all waves present in the wave spectrum. A realistic transient and spatially dependent velocity field may then be reconstructed from a linear sum of the spectral components given in Eqs. 17 and 18. For example, the normal velocity is given by

$$v'(x, y, t) = \sum_{j=1}^{N} \beta_j(x, t) y \tag{31}$$

where β_j is obtained from Eq. 21 and N is the total number of modes in the spectrum. Statistical properties of this reconstructed transient velocity field may then be scrutinized.

Figure 5 shows the magnitudes of the complex-valued spectral density functions for wave amplitude, $|\Phi_a(f)|$, and the reconstructed time-varying part (β) of the normal velocity, $|\Phi_\beta(f)|$. The spectral estimates of Figure 5b should be viewed as having a one-to-one correspondence with each point in Figure 5a; each point in Figure 5b is derived from Eqs. 14 and 15 utilizing the wave parameter set corresponding to the wave spectral set $\{f, |\Phi_a(f)|\}$. The effective hydrodynamic frequencies [i.e., large $|\Phi_\beta(f)|$] are shown to be neither high nor low wave frequencies, but rather some intermediate frequency. These effective waves typically have a wavelength of about 1 cm, and an Eulerian frequency of 10–30 Hertz. The spectrum of β will be described by a variance $\underline{\beta}^2$, given as

$$\underline{\beta}^2 = \int_0^\infty |\Phi_\beta(f)|\, df. \tag{32}$$

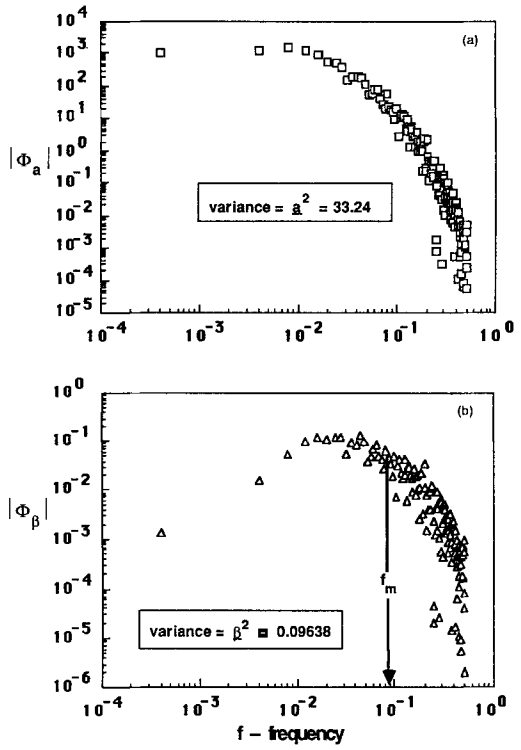

Figure 5. Typical spectral density functions.
(a) Measured wave amplitude
(b) Time variation of the normal velocity β computed from Eq. 21 using wave amplitude-frequency sets

Our calculations of average mass transfer coefficients for gas-liquid interfaces have indicated that the frequency content of the velocity field acts through a characteristic frequency that for practical purposes is the median of the frequency domain. It is noted that this is not a general result. The characteristic frequency may be a much more complex function for other flow situations. The median frequency, f_m, is defined as

$$f_m = \int_0^\infty f|\Phi_\beta|\, df/\underline{\beta}^2 \tag{33}$$

and will essentially represent a weighted range of dominant frequencies. As mentioned previously, numerical solutions reveal that the normal velocity component is of dominant importance to mass transfer. Consequently, the values of $\underline{\beta}^2$ and f_m may be viewed as the hydrodynamic statistical variables of greatest importance when examining gas-liquid interfacial mass transport.

Finite difference solutions

For highly convective flows, convective scalar terms in mass (or heat) balances are generally represented with finite difference schemes involving *upwind differences*. This class of difference schemes stabilizes solutions, transports mass in the direction of convection (transportive property), and increases the speed of solution convergence. Diffusive terms are represented by centered differencing, which is second-order accurate in space, and the temporal term of Eqs. 6 and 7 is forward-differenced so as to produce an implicit algebraic equation. Implicit

schemes are unconditionally stable by nature and require solutions of tridiagonal matrices to advance the time level.

Past numerical analyses of mass transfer at solid-liquid interfaces by Campbell and Hanratty (1983) and McCready et al. (1986) involved upwind difference schemes for convective terms of Eqs. 6 and 7, which were first-order accurate in space, and did not possess the *conservative property*. As discussed by Roache (1972), a scheme posseses the conservative property if integral conservation relations of the continuum equations are preserved. It is this property that is found to have the most consequential effects on the numerical solutions of the advection-diffusion equation. In this study, an upwind difference scheme sometimes called the "second upwind difference" or "donor cell" is used for convective terms. This scheme possesses the conservative property, and is pseudosecond-order accurate in space for regions where scalar gradients are small. This scheme for some scalar ψ, velocity W, and space coordinate Z is implemented at an arbitrary grid point i as follows:

$$\left[\frac{\partial(\psi W)}{\partial Z}\right]_i = \frac{\psi_R W_R - \psi_L W_L}{\Delta Z} \tag{34}$$

with

$$W_R = (W_{i+1} + W_i)/2$$
$$W_L = (W_{i-1} + W_i)/2$$

and

$$\psi_R = \psi_i \text{ if } W_R > 0, \quad \psi_R = \psi_{i+1} \text{ if } W_R < 0$$
$$\psi_L = \psi_i \text{ if } W_L < 0, \quad \psi_L = \psi_{i-1} \text{ if } W_L < 0$$

If, for example, the concentration field is slowly varying with W_R and W_L greater than zero, then $\psi_R = \psi_L = \psi$, and Eq. 34 reduces to

$$\left[\frac{\partial(\psi W)}{\partial Z}\right]_i = \frac{\psi}{2\Delta Z}\{W_{i+1} - W_{i-1}\} \tag{35}$$

which is second-order accurate in the convective field. The *unconservative* upwind difference scheme used by Campbell and Hanratty (1983) and McCready et al. (1986) unrealistically produces "zero" convection in regions of a slowly varying scalar, $\partial\psi/\partial Z \to 0$. The scheme implemented for the convective term of Eq. 34 by these investigators has the form:

$$\left[\frac{\partial(\psi w)}{\partial z}\right]_i = \left(\frac{\partial\psi}{\partial z}\right)_i w_\epsilon \tag{36}$$

where w_ϵ is some average velocity about the grid point i, with ϵ taken as $i \pm 1$, depending on the direction of the upwind at the particular time step. If the concentration field is slowly varying, Eq. 36 approaches zero. Therefore, no convection will exist in the solution scheme if the concentration gradient is small and diffusion will tend to smooth out these gradients. Our numerical work has shown that Eq. 10 or 11 cannot be satisfied if the convective term representation of Eq. 36 is used because convection is prevented from dominating in regions where the concentration gradient is small. For example, near $y = \delta_c$ it is physically reasonable that convection should dominate since $\partial c/\partial y \approx 0$. However, the use of Eq. 36 will not allow this to occur. Even if the concentration difference between grid points is small and little concentration change occurs due to the local convective flow, the numerical formulation must allow mass to be convected or the physical picture assumed when an upwind scheme is used will be violated.

Solutions of Eq. 7a and Eqs. 6b and 6c involve the evaluation of one tridiagonal matrix at each time step. For a typical one-dimensional computation, 100 normal direction divisions, and a maximum of 10,000 time steps were required to insure statistical and spatial convergence of the concentration field. To satisfy Eq. 11, it was necessary to iterate on the assumed value of δ_c. This proved to be a straightforward task. If δ_c was too small, the convective flux was less than the diffusive flux and further decreasing δ_c would make the diffusive flux even larger and the convective flux lower. Alternatively, if the value of δ_c was chosen too large, the convective flux exceeded the diffusive flux and if δ_c was increased further, the diffusive flux would decrease and the convective flux increase. It was found that all of the boundary conditions and Eq. 11 could be satisfied at only one value of δ_c for each set of experimental variables.

For solutions of Eqs. 6a–6e, the alternating-direction-implicit (ADI) method of Peaceman and Rachford (1955) is used. This method avoids iterative solutions of a pentadiagonal matrix by splitting the time step between two subordinate mass balance equations. Time advancement then requires the solution of two tridiagonal matrices. For statistical convergence of the transient and spatial concentration field in Eqs. 6a–6e, 100 normal direction and 50 tangential direction divisions are used, along with a maximum of 4,000 time steps. The CPU time required for a two-dimensional solution was approximately 10 times that consumed for a one-dimensional calculation when using the same machine. Variations of first and second kind boundary conditions for Eqs. 6d and 6e were found to have negligible effect on the computed concentration field. The value of x_L used in computations was taken as 10^3. This value was chosen so that the concentration and hydrodynamic scales from the largest and smallest wavelength waves on the surface were resolvable and unsmoothed. Values of x_L that satisfied this criteria had an insignificant effect on computed mass transfer rates.

The time increment, Δt, for both one- and two-dimensional solutions was chosen so as to fulfill the Nyquist criterion for the highest frequency found in the reconstructed velocity spectrum. Thus,

$$\Delta t = \frac{1}{2 f_{\max}} \tag{37}$$

where $f_{\max}$ is the maximum dimensionless frequency of the wave amplitude or velocity field spectrum. In Figure 5, $f_{\max}$ would be roughly 0.5, so that Δt would be approximately 1.0. Dimensionally, this corresponds to a time step of 3.6×10^{-3} s. All statistical evaluations of the transient fields were performed with IMSL FFT subroutines.

Statistical and averaged behavior of solutions to one- and two-dimensional equations

Understanding the effect of hydrodynamics on interfacial mass transport reduces to an analysis of the statistical properties of the velocity field and mass transfer coefficient. The important

hydrodynamic statistical properties are $\underline{\beta}^2$ and f_m, defined by Eqs. 32 and 33. The most important statistical property of the mass transfer coefficient is the time average of Eq. 4 defined as K. Other significant properties of $k(t)$ are its mean frequency

$$f_k = \int_0^\infty f|\Phi_k|\, df/\underline{k}^2 \tag{38}$$

where $|\Phi_k(f)|$ and $\underline{k}^2$ are the spectral density function and variance of $k(t)$, respectively and the intensity of mass transfer rate fluctuations

$$k_i = \frac{\{\underline{k}^2\}^{1/2}}{K}. \tag{39}$$

Based on continuity arguments, it would be expected that the term $\partial\langle u'c\rangle/\partial x$ would be of the same order of magnitude as $\partial\langle v'c\rangle/\partial y$. However, numerical simulations done by Campbell and Hanratty (1983) demonstrate that a one-dimensional model equation, which contains only normal direction convection gives essentially the same behavior as the two-dimensional equation for the calculation of average transfer coefficients. Since the justification for using a one-dimensional equation cannot be that one convective term is smaller than the other, another explanation must be sought. Figure 6 displays instantaneous tracings for $\partial\langle u'c\rangle/\partial x$ and $\partial\langle v'c\rangle/\partial y$ at an interior grid point, $x/x_L = 0.58$ and $y/\delta_c = 0.49$. As expected, the instantaneous magnitudes of these convective terms are similar. However, it is the x-space average of the integral over δ_c that is important in determining the average mass transfer rate [x-space average of $K(x)$ in Eq. 10]. The x-space averages of the first and second terms on the righthand side of Eq. 10 are 7.216×10^{-3} and 1.404×10^{-4}, respectively. It is noted that the magnitude of the third term on the righthand side of Eq. 10 is 1.597×10^{-8}, which contributes negligibly to overall mass transport in the layer. These values reveal that the net mass flux contribution over the domain from the $\partial\langle u'c\rangle/\partial x$ term is at least a factor of 50 smaller than the contribution from $\partial\langle v'c\rangle/\partial y$. Although $\partial\langle u'c\rangle/\partial x$ may contribute to mass convection at a given point in the flow field, this term does very little in the overall mass transport process. One may then conclude that the use of a one-dimensional advection-diffusion equation in mass transfer studies is valid for determination of transfer rates because the important mass transfer physics are contained in this normal-direction equation.

As expected, the transient behavior of $k(t)$ is very similar for one- and two-dimensional calculations. Figure 7 compares the nature of $k(t)$ from one- and two-dimensional solutions using equivalent velocity fields. Spectra of these temporal tracings are shown in Figure 8. It is obvious from the tracings of Figure 7 that $k(t)$ does not respond equivalently to all frequencies of $\beta(t)$, since f_k is about 40% of f_m. In other words, the most dominant mass transfer coefficient fluctuations have a frequency content that is about 40% of the most dominant normal velocity fluctua-

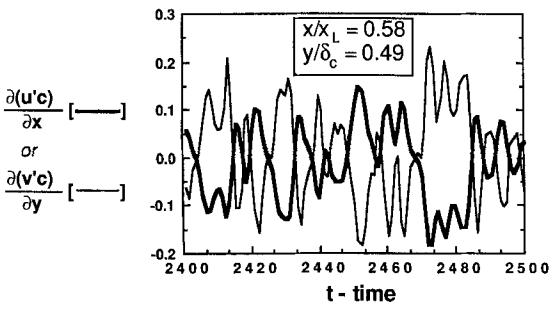

Figure 6. Instantaneous magnitudes of convective terms in 2-D advection-diffusion equation for mass, Eq. 6a.

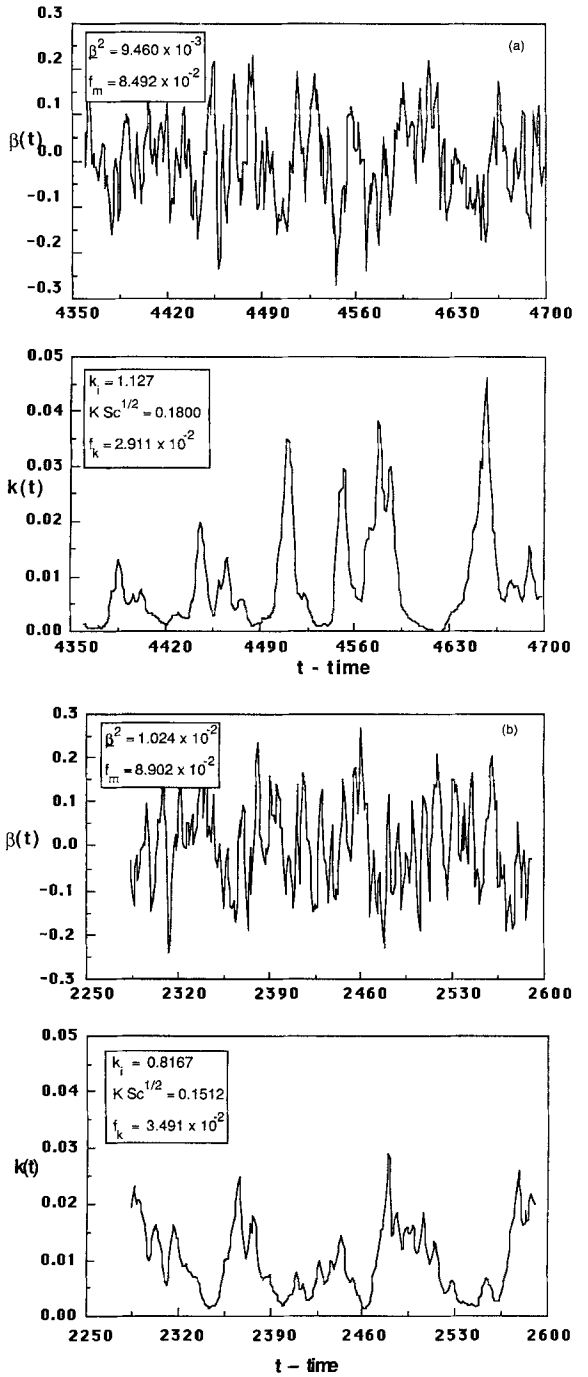

Figure 7. Instantaneous normal velocity gradient β and resultant instantaneous mass transfer coefficients k.

Figure 7a. 1-D calculation using Eqs. 4 and 7a.

Figure 7b. 2-D calculation using Eqs. 4 and 6a.

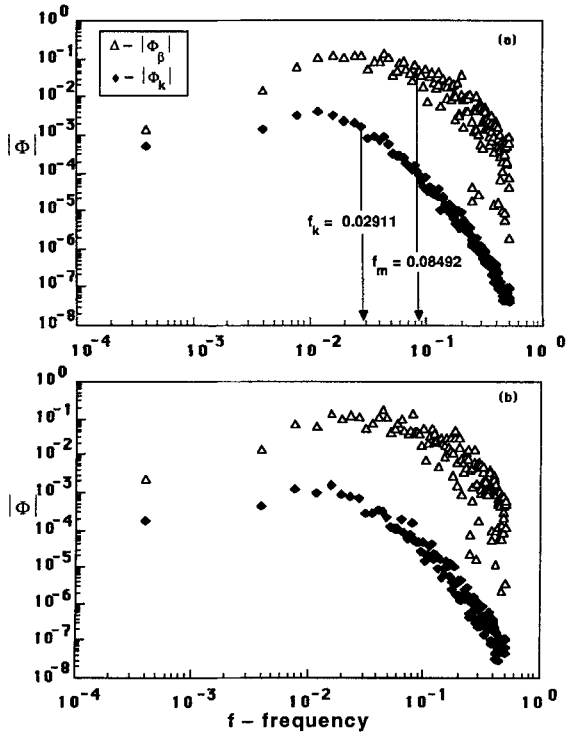

Figure 8. k and β spectra.
(a) 1-D computation of Figure 7a
(b) 2-D computation of Figure 7b

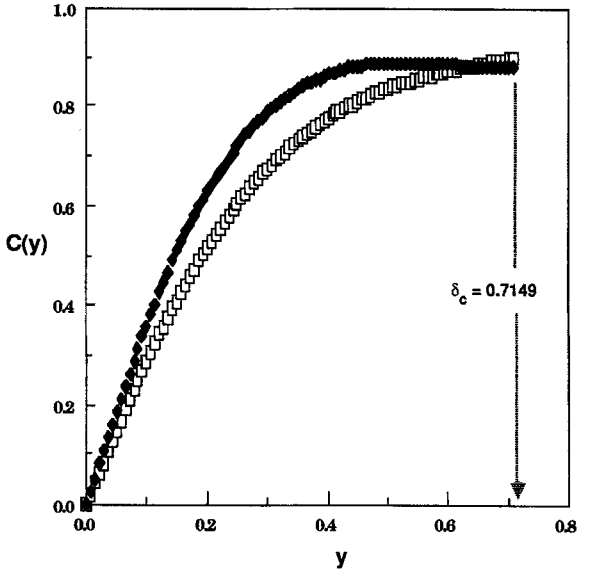

Figure 9. Mean concentration profiles.
□ 1-D advection-diffusion equation; ♦ 2-D advection-diffusion equation

tions. As is evident from Figures 7 and 8, $k(t)$ responds most dramatically to low-frequency components of the normal velocity component, $\beta(t)$. If all hydrodynamic frequencies were equally effective, the spectral density functions $|\Phi_k(f)|$ and $|\Phi_\beta(f)|$ would be of similar shape. Figure 8 shows the dissimilar nature of these functions for $f > 0.02$ where the spectra of the mass transfer coefficients are seen to decay more rapidly than that of the velocity gradient. Details about the effectiveness of various hydrodynamic scales will be discussed in a later paper. Figure 7 depicts a clear correlation between maximum normal velocity inflows ($\beta < 0$) and a peak in the mass transfer rate. This is interpreted as a steepening of concentration profiles as bulk fluid at concentration $c = 1$ penetrates toward the surface. As fluid retreats from the interface, the concentration gradient relaxes and the mass transfer rate decreases. In Figure 7, the average mass transfer rate $[K]$, k_i, and f_k for each are also shown, and are nearly equivalent to one- and two-dimensional solutions. The major differences are for k_i, which is observed to be qualitatively smoother due to the effect of tangential convection.

Figure 9 illustrates the general appearance of the mean concentration profiles computed from the one- and two-dimensional advection-diffusion equations. For the two-dimensional solution, this is the mean concentration profile in y averaged over all x locations. These profiles are shown for a value of δ_c where convective and diffusive transport are matched (Eq. 10 and x-space average of Eq. 11). It is reasonable to expect that some difference in appearance will exist between one- and two-dimensional solutions. The spatial region of major difference would intuitively be that in the outer region of δ_c where hydrodynamics have a much more influential role. This tangential "smoothing" or "mixing" effect on $C(y)$ is observed in Figure 9, where $C(y)$ from the two-dimensional calculation is less steep for large y. It should also be noted that a time-averaged value for $C(\delta_c)$, for both one- and two-dimensional solutions, that does not equal 1 is expected and is consistent with the present formulation. The location of δ_c will be at the point where the concentration gradient is nearly zero and the convective flux has a value equal to the wall flux. Because of boundary condition Eq. 6c, the value of the time-averaged concentration at this point is determined by inflows where $c(\delta_c) = 1$ and outflows that have a somewhat lower concentration.

Another possible boundary condition would be for $c(\delta_c) = 1$ for an inflow and outflow, thus fixing the concentration at the outer boundary. This, however, does not allow for $\partial c/\partial y \approx 0$ at $y = \delta_c$, and consequently Eq. 10 or 11 cannot be satisfied. Since it is physically reasonable that the shape of the concentration field will be quite different for an inflow (resulting in a very steep gradient) and an outflow (resulting in a nearly gradientless profile), boundary condition Eq. 6c allows for more freedom in this variation since $c(\delta_c)$ is not forced to be 1 for an outflow.

Comparison with Experiments

Using wave amplitude spectra obtained from experiments in a gas-liquid flow system by McCready (1984) and McCready and Hanratty (1985), mass transfer rates are computed from Eqs. 6 and 7, with Eqs. 21 and 22 in Eqs. 14 and 15, respectively. The results are compared to the correspondingly measured mass transfer coefficients of McCready and Hanratty (1985). It is worth repeating that these computed rates are calculated directly from wave amplitude spectra using only measured hydrodynamic variables. Figure 10 shows a comparison of numerical and experimental $K\,Sc^{1/2}$ values for two different gas Reynolds numbers for water and 20 wt. % glycerine/water films. Both one- and two-dimensional results are shown in Figure 10a to illustrate the small difference that results from the

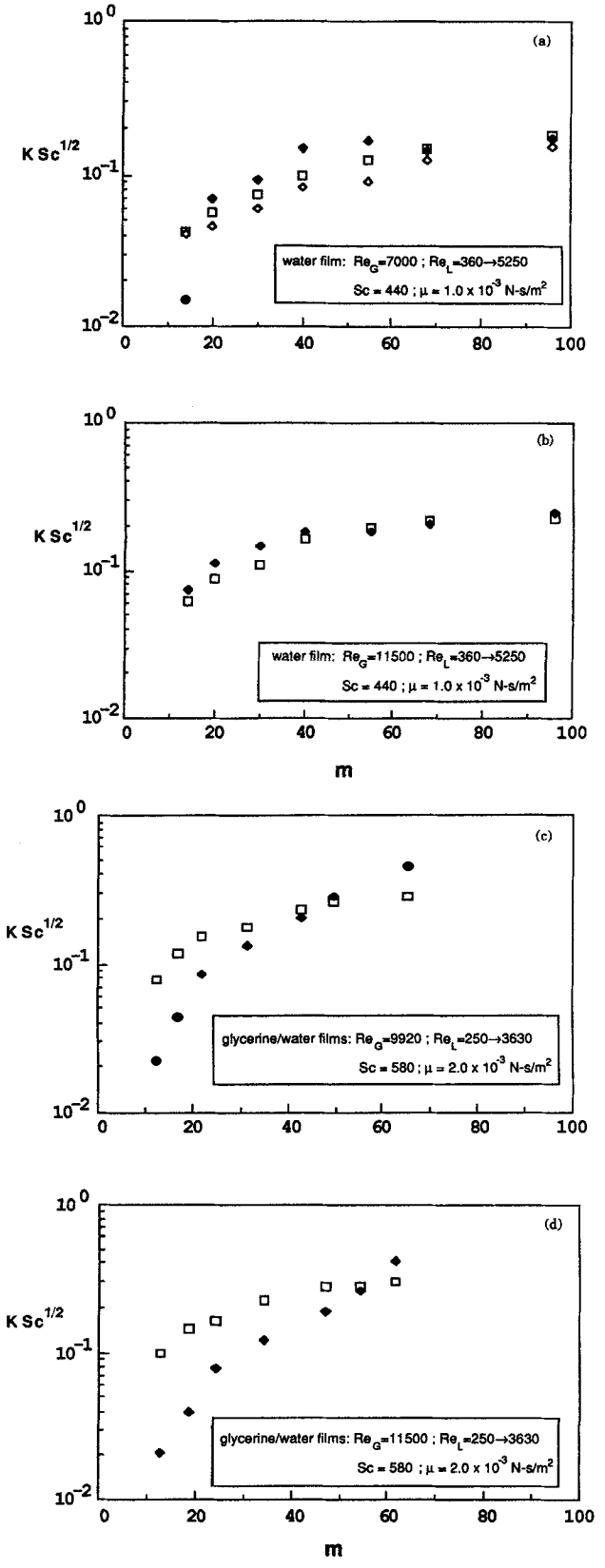

Figure 10. Numerical and experimental mass transfer coefficient comparison over a range of film thicknesses.

♦ experimental values; □ 1-D numerical computations; ◇ 2-D numerical computations

use of the simplified equation. Figures 10b, 10c, and 10d are further comparisons of experimental mass transfer coefficients with one-dimensional finite-difference solutions.

For the cases where water is the liquid, the predicted mass transfer rates are generally within 50% of the measured ones and often much better. We note that as expected, the well-mixed model cannot predict the sharp drop that occurs as m is decreased, and the film could be described as being in regions II or III of Figure 2. In Figure 10a the calcuation predicts values of the mass transfer coefficient that are a factor of 3 too large for very small m.

Values of K for glycerine/water films are found experimentally to be much larger than those for pure water films and to always increase with m (for a more comprehensive display of experimental data see McCready and Hanratty, 1985). For the range of available experimental conditions, these films can probably always be categorized as being in regions II or III. The numerical calculations correctly predict larger values for K than for water and as expected, cannot predict the fast decrease in K with m.

The magnitude of measured mass transfer coefficients to thinner films can be explained from the eigenvalue solution given earlier in the section on interfacial mass transport for laminar films. In Figure 11, experimental K's are compared to analytic solutions for experimental conditions from Figure 10 which approximately satisfy the laminar flow assumptions. These solutions predict $K\,Sc^{1/2}$ to fall somewhere between 1.0×10^{-2} and 2.0×10^{-2}, which is in the range of measured rates and about an order of magnitude smaller than for thicker films.

Discussion

The results presented above provide evidence from which to determine both the overall picture of mass transfer to a sheared liquid film and the specific mechanism that is of dominant importance in causing the effective velocity fluctuations. Previously, McCready and Hanratty (1985) had explained the drop in their mass transfer coefficients for thinner films qualitatively in terms of a change in the wave parameters. However, the calculations presented here show that while there is a decrease in the mass transfer rates expected for thinner films due to a lessening of effective wave energy, this effect alone cannot explain the large magnitude of the drop. Quite clearly, the level of mixing of the bulk film must decrease due to the diminishing level of bulk turbulence with film thickness and Reynolds number so that eventually the mass transfer resistance is not confined to a thin surface region but pervades the entire film. It is seen that the mass transfer coefficients calculated for purely laminar flow provide a good estimate of the lower limit of the transfer rates. To explain quantitatively the behavior that occurs between the fully mixed and laminar limits, region II, a numerical solution of Eq. 3 for the entire film with an accurate description of the effects of waves on the flow field is needed.

Good agreement with measured mass transfer coefficients alone is not sufficient grounds to justify the calculation procedure. Two questions remain: How accurate is the representation of the flow field? And is the definition of the solution domain for mass transfer calculations correct? For the first of these questions we must rely on the linearity of the advection-diffusion equation and the equation governing the flow field very near the interface. The largest wave slopes are less than 10^{-1} and typically are of the order 10^{-2}. As a consequence, the flow field

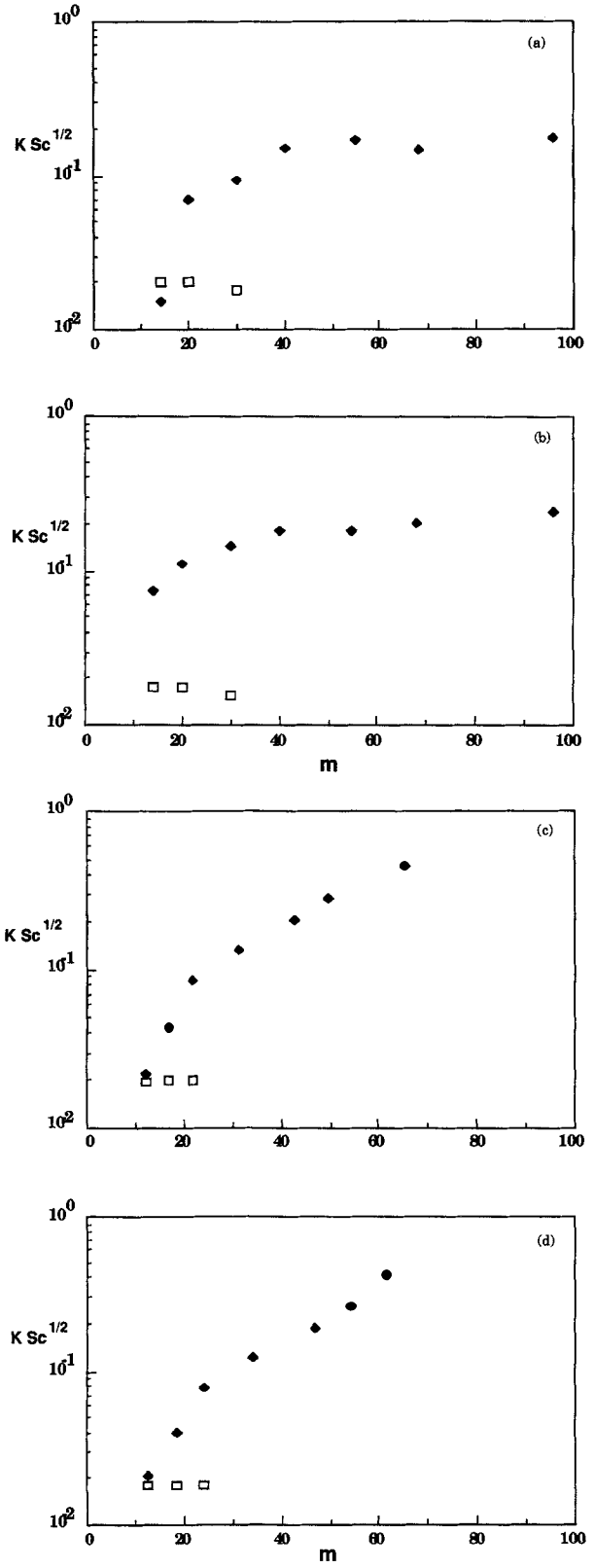

Figure 11. Analytical and experimental mass transfer coefficient comparison over a range of film thicknesses.

♦ experimental values; □ analytical solutions
Experimental flow conditions of (a)–(d) correspond to flow conditions of Figure 10a–10d, respectively

within the waves should be well represented by the Orr-Sommerfeld equation. Because the region over which the velocity field is needed is so thin (for typical experimental conditions δ_c is about 0.1 mm), inertial effects should be negligible and it is reasonable to expect that the flow field is accurately represented by the linear superposition of all present wave components. We note that this would not be true far away from the interface, where turbulence is important and where inertial effects associated with waves would be strong. Secondly, the advection-diffusion equation is linear, so its time-averaged solutions are determined by the statistical properties of the forcing velocity field and boundary conditions, not by any initial conditions or specific instantaneous behavior of the velocities as might be expected for nonlinear equations. Consequently, a velocity field that can be used to accurately compute average mass transfer coefficients must have only the correct behavior for the important statistical variables, β^2 and f_m. This makes reconstruction of an accurate velocity field possible.

It is necessary to limit the solution domain if any quantitative predictions of mass transfer rates are to be achieved unless the entire velocity field within the film is known accurately. For the present problem, the average layer thickness can be defined if the velocity field is known accurately for the entire region where transfer resistance occurs. Solution of Eq. 3 for values of y beyond this point will reveal no further information about the mass transfer problem. For this formulation to be correct, it is necessary that the convection due to the Orr-Sommerfeld velocity field remain sufficiently large (at least as big as its value at δ_c) until a distance at which turbulent velocity fluctuations would be expected to provide an even greater degree of mixing. The qualitative trend in the experimental data suggests that this does happen for sufficiently thick films. For thinner films adequate turbulent mixing does not occur, leading to additional resistance to transfer not included in the formulation. Consequently, predictions of transfer coefficients do not decrease sufficiently rapidly as the film thickness is decreased.

Use of Eq. 10 or 11 to determine δ_c makes the numerical simulation method self-consistent and will allow evaluation of mass transfer rates that would result for any arbitrary velocity field either at a mobile interface or a solid wall. Other suspect mechanisms (e.g., turbulence produced near the interface or fluctuations caused by surface flexing) may be investigated by the methods outlined in this paper. Tracings shown in Figure 7 and the spectra of Figure 8 indicate that the degree of mass transfer is controlled by the magnitude and frequency of the velocity fluctuations normal to the interface. The magnitudes of $\underline{\beta}^2$ caused by shear stress variations due to the interaction of waves and the turbulent gas flow are large enough and f_m is in the correct range to produce the observed rates. At the very least, the description proposed by McCready and Hanratty (1985) must be a codominant hydrodynamic mechanism. A greater degree of accuracy in the description of the hydrodynamics of the interfacial region could be achieved by the addition of a third dimension in the Orr-Sommerfeld analysis or the inclusion of nonlinear terms. However, given the present good agreement between measurements and calculations, this additional effort does not appear to be warranted at least until the time when accurate hydrodynamic measurements of the region near the interface are available.

An interesting contribution of the numerical approach is the insight gained about the transient nature of mass transport,

which has not emerged in past turbulence studies involving eddy diffusivities that attempt to relate mass transport rates to integral or mean time scales of the entire flow field. As illustrated in Figures 7 and 8, not all scales are effective in producing mass transfer. While use of integrals or averages of the *effective* scales will give accurate quantitative values for the average transfer rates, the physical description of the transfer process would still be obscured because its full transient nature could not be observed.

Acknowledgment

The authors thank the Engineering Foundation for partial financial support for this research through Grant No. RI-A-85-14, and the National Center for Supercomputing Applications for computational time for a portion of the calculations.

Notation

Except as explicitly noted, all variables are dimensionless with the kinematic viscosity ν and the interfacial liquid-side friction velocity v^*.

a = wave amplitude
$\underline{a^2}$ = variance of surface-wave height variation
A_k = constants in Orr-Sommerfeld equation solution, Eq. 19 (k = 1, 4)
$\mathcal{A}$ = denotes solute species in liquid
ADI = acronym for Alternating-Direction-Implicit
B_k = eigenconstants in series solution, Eq. 25 ($k = 1, \infty$)
c = dimensionless concentration, $c = (c_d - c_{d,b})/c_d^* - c_{d,b})$
C = time-averaged part of concentration
c' = fluctuating part of concentration
c_0 = initial concentration profile $c_0 = c_0(\eta)$, Eq. 24a
c_d = concentration, kg · m^{-3}
$c_{d,b}$ = bulk concentration, kg · m^{-3}
c_d^* = interfacial concentration, kg · m^{-3}
D = molecular diffusivity of $\mathcal{A}$ in liquid, m^2 · s^{-1}
f = frequency
f_c = characteristic frequency or range of frequencies in velocity field
f_k = mean frequency of $k(t)$, Eq. 38
f_m = mean frequency $\beta(t)$, Eq. 33
$f_{\max}$ = maximum frequency used in wave amplitude of velocity spectra
F = variable that satisfies two-dimensional continuity, used to derive Orr-Sommerfeld eq., Eqs. 17 and 18
FFT = acronym for Fast-Fourier-Transform
G_3 = complex function, Eq. 19
G_4 = complex function, Eq. 19
H = average heat transfer coefficient, Eq. 2
H_k = eigenfunctions in solution to Eq. 23
$i = (-1)^{1/2}$
k = mass transfer coefficient
K = time-averaged mass transfer coefficient, Eq. 11 or space average of Eq. 10
$K(x)$ = spatial time-averaged mass transfer coefficient, Eq. 10
k_i = intensity of mass transfer coefficient, Eq. 39
$\underline{k^2}$ = variance of mass transfer coefficient fluctuations
m = film thickness
Pe = Peclet number, $Pe = Sc\,U(0)m$
Pr = Prandtl number; $Pr = \nu/D_t$, D_t is the molecular thermal diffusivity
q = defined from $q^2 = -i\alpha\chi$
Re_L = liquid Reynolds number based on four times the film thickness; $Re_L = 4U_f m/v$, U_f is the average dimensional film velocity
Re_G = gas Reynolds number
s = defined from $s^2 = -i\alpha[\chi - U(0)]$
Sc = Schmidt number defined as ν/D
SSV = acronym for Shear-Stress-Variation
t = time
$\boldsymbol{u}$ = three-dimensional velocity vector
u = tangential velocity
U = mean component of tangential velocity
u' = fluctuating component of mean velocity
$U(0)$ = mean component of tangential velocity evaluated at interface
v = normal velocity
v' = fluctuating component of normal velocity
v^* = interfacial liquid-side friction velocity $v^* = (\tau/\rho_L)^{1/2}$, m · s^{-1}
w = transverse velocity
W = arbitrary velocity, Eqs. 34–36
W_R = "right side" average of W, Eq. 34
W_L = "left side" average of W, Eq. 34
x = tangential direction coordinate
x_L = value of x in numerical solution domain size, Eq. 6e
y = normal direction coordinate
z = transverse direction coordinate
Z = arbitrary length coordinate, Eqs. 34–36

Greek letters

α = wave number, $2\pi/\lambda$
β = t and x varying part of normal velocity, Eq. 21
$\underline{\beta^2}$ = variance of β
χ = Eulerian reference frame wave speed
δ_c = concentration boundary layer thickness
δ_h = hydrodynamic boundary layer thickness
ϵ = subscript in grid point location, Eq. 36
Φ_a = complex-valued spectral density function for a
Φ_β = complex-valued spectral density function for β
Φ_k = complex-valued spectral density function for k
γ = t and x varying part of tangential velocity
η = normal direction coordinate variable, $(1 - y/m)$, Eq. 23
λ = wavelength
λ_k = eigenvalues in series solution of Eq. 23
μ = function, Eq. 28
μ_L = viscosity of liquid, N · s · m^{-2}
ν = kinematic viscosity of liquid, m^2 · s^{-1}
θ = independent variable of Airy functions, Eq. 27
ρ_L = liquid density, kg · m^{-3}
τ = dimensional mean shear stress at interface, N · m^{-2}
τ' = fluctuating shear stress at interface
$\tau(0)$ = amplitude of fluctuating shear stress at interface
Ψ = arbitrary scalar variable, Eqs. 34–36
Ψ_R = "right side" value of Ψ, Eq. 34
Ψ_L = "left side" value of Ψ, Eq. 34
ζ = tangential direction coordinate variable, x/m, Eq. 23

Mathematical operations

Ai, Bi = Airy functions of argument θ
Ai', Bi' = derivatives of Airy functions of argument θ
$f[\ ]$ = a function
$\langle\ \rangle$ = a time-averaged product enclosed
$O(y^2)$ = functions of order y^2 or larger which decay to "0" as $y \to 0$
∇ = vector operator $\partial/\partial x$
∇^2 = vector operator $\partial^2/\partial x^2$
Δ = linear difference operator
$|\ |$ = magnitude of complex function
Real $[\ ]$ = real part of a complex function
$\approx$ = approximately equal to
$\to$ = asymptotically approaches

Literature Cited

Abrams, J., and T. J. Hanratty, "Relaxation Effects Observed for Turbulent Flow Over a Wavy Surface," *J. Fluid Mech.*, **151**, 443 (1985).

Aisa, L., B. Caussade, J. George, and L. Masbernat, "Exchange of Gas in Stratified Gas-Liquid Flows," *Int. J. Heat Mass Transfer*, **24**, 1005 (1981).

Back, D. D., and M. J. McCready, "Effect of Small-Wavelength Waves on Gas Transfer Across the Ocean Surface," *J. Geophys. Res.*, **93**(C5), 5143 (1988).

Brodkey, R. S., K. N. McKelvey, H. C. Hershey, and S. G. Nychas,

"Mass Transfer at the Wall as a Result of Coherent Structures in a Turbulently Flowing Liquid," *Int. J. Heat Mass Transfer,* **21,** 593 (1978).

Campbell, J. A., and T. J. Hanratty, "Mechanism of Turbulent Mass Transfer at a Solid Boundary," *AIChE J.,* **29,** 221 (1983).

Caussade, B., and A. Souyri, "Wind-Generated Turbulence in Stratified Flow," *Advancements in Aerodynamics, Fluid Mechanics, and Hydraulics,* Am. Soc. Civil Engineers (1986).

Chung, D. K., and A. F. Mills, "Experimental Study of Gas Absorption into Turbulent Falling Films of Water and Ethylene Glycol-Water Mixtures," *Let. Heat Mass Transf.,* **1,** 43 (1974).

Cohen, L. S., and T. J. Hanratty, "Generation of Waves in the Concurrent Flow of Air and a Liquid," *AIChE J.,* **11,** 138 (Feb., 1965).

Fabre, J., D. Marodon, L. Masbernat, and C. Suzanne, "Turbulence Structure of Wavy Stratified Air-Water Flow," *Gas Transfer at Water Surfaces,* Reidel Pub. Co., 113 (1984).

Gastel, K. van, P. A. E. M. Janssen, and G. J. Komen, "On Phase Velocity and Growth Rate of Wind-Induced Gravity-Capillary Waves," *J. Fluid Mech.,* **161,** 199 (1985).

Hanratty, T. J., "Interfacial Instabilities Caused by Air Flow Over a Thin Liquid Layer," *Waves on Fluid Interfaces,* Academic Press, New York (1983).

Henstock W. H., and T. J. Hanratty, "Gas Absorption by a Liquid Layer Flowing on the Wall of a Pipe," *AIChE J.,* **25,** 122 (1979).

Jensen, R. J., and M. C. Yuen, "Interphase Transport in Horizontal Stratified Cocurrent Flow," *U.S. Nuclear Regulatory Commission,* NUREG CR-2334 (1982).

Kasturi, G., and J. B. Stepanek, "Two-Phase Flow: IV. Gas and Liquid Side Mass Transfer Coefficients," *Chem. Eng. Sci.,* **29,** 1849 (1974).

Mattingly, G. E., "Experimental Study of Wind Effects on Reareation," *J. Hydraulics Div. ASCE,* **95**(HY1), 577 (1977).

McCready, M. J., "Mechanism of Gas Absorption at a Sheared Gas-Liquid Interface," Ph.D. Thesis, Univ. Illinois, Urbana (1984).

McCready, M. J., and T. J. Hanratty, "Effect of Air Shear on Gas Absorption by a Liquid Film," *AIChE J.,* **31,** 2066 (1985).

McCready, M. J., E. Vassiliadou, and T. J. Hanratty, "Computer Simulation of Turbulent Mass Transfer at a Mobile Interface," *AIChE J.,* **32,** 1108 (1986).

Peaceman, D. W., and H. H. Rachford, Jr., "The Numerical Solution of Parabolic and Elliptic Differential Equations," *J. Soc. Indust. Appl. Math.,* **3,** 28 (1955).

Polhausen, K. Z., *Angew, Math. Mech.,* **1,** 252 (1921).

Roache, P. J., *Computational Fluid Dynamics,* Hermosa, Albuquerque, Ch. 3, (1972).

Rotem, Z., and J. E. Neilson, "Exact Solution for Diffusion to Flow Down an Incline," *Can. J. Chem. Eng.,* **47,** 341 (1969).

Squire, H. B., "On the Stability for Three-Dimensional Disturbances of Viscous Fluid Flow Between Parallel Walls," *Proc. Roy. Soc.* **A, 142,** 621 (1933).

Stewart, W. E., "Forced Convection in Three-Dimensional Flows. I: Asymptotic Solutions for Fixed Interfaces," *AIChE J.,* **9,** 528 (1963).

———, "Forced Convection. IV: Asymptotic Forms for Laminar and Turbulent Transfer Rates," *AIChE J.,* **33,** 2008 (1987).

Stewart, W. E., J. B. Angelo, and E. N. Lightfoot, "Forced Convection in Three-Dimensional Flows. II: Asymptotic Solutions for Mobile Interfaces," *AIChE J.,* **16,** 771 (1970).

Stewart, W. E., and M. A. McClelland, "Forced Convection in Three-Dimensional Flows. III: Asymptotic Solutions with Viscous Heating," *AIChE J.,* **29,** 947 (1983).

Thorsness, C. B., P. E. Morrisroe, and T. J. Hanratty, "A Comparison of Linear Theory with Measurements of the Variation of Shear Stress Along a Solid Wave," *Chem. Eng. Sci.,* **33,** 579 (1978).

Manuscript received Mar. 21, 1988, and revision received June 13, 1988.